QUARTERLY JOURNAL OF THE ROYAL METEOROLOGICAL SOCIETY
Q. J. R. Meteorol. Soc. **135**: 880–893 (2009)
Published online 6 April 2009 in Wiley InterScience
(www.interscience.wiley.com) DOI: 10.1002/qj.411

The dynamics of a polar low assessed using potential vorticity inversion

Thomas J. Bracegirdle* and Suzanne L. Gray
The University of Reading, Reading, UK

ABSTRACT: The dynamics of a polar low are examined using a piecewise potential vorticity (PV) inversion method. In previous studies of this and other polar lows, structural evolution has been described in terms of regions of anomalous PV. In this study the relative importance of different PV anomalies and the interactions between them have been quantified using PV diagnostics. The intensification of the polar low occurred in three stages (in contrast to previous studies of polar lows that have only identified two stages). The dynamical characteristics of stages one and two are consistent with the proposed type C cyclogenesis mechanism. A diabatically-generated lower-tropospheric PV anomaly dominated intensification after initial triggering by a positive upper-level PV anomaly. A phase tilt between the upper and lower levels was maintained through retardation of the positive upper-level anomaly by the effects of latent heat release. Stage three was a period of growth dominated by wind-induced surface heat exchange (WISHE), which contributed at least 18% to the amplitude of the mature surface polar low. Copyright © 2009 Royal Meteorological Society

KEY WORDS cyclone; case-study; attribution

Received 7 October 2008; Revised 27 January 2009; Accepted 2 February 2009

1. Introduction

Potential vorticity (PV) diagnostics have been used extensively to gain a better understanding of the life cycles of cyclonic storms through case-studies and idealised simulations (e.g. Hoskins *et al.* 1985; Davis and Emanuel, 1991; Stoelinga, 1996; Huo *et al.*, 1999; Plant *et al.*, 2003; Agusti-Panareda *et al.*, 2004; Ahmadi-Givi *et al.*, 2004). The results of these studies have contributed to the introduction of new conceptual models of cyclogenesis. However, their focus is mainly on extratropical cyclones and hurricanes. There are still significant uncertainties in the relative importance of different mechanisms that contribute to the intensification of polar lows; polar lows are defined as intense mesoscale cyclones (200 to 1000 km in diameter) that often occur in cold air masses that move over relatively warm ocean surfaces at high latitudes (Rasmussen and Turner, 2003). For instance, is the role of latent heat release similar to that seen in strongly convective midlatitude cyclones? What is the relative importance of baroclinic versus non-baroclinic processes? Here we use PV diagnostics to answer these questions for a polar low that occurred over the Norwegian Sea on 13 October 1993 (referred to as the PL in the rest of this paper).

Observations and numerical simulations of polar lows have shown that intensification can often be conceptualised in two stages: an initial baroclinic stage followed by a stage dominated by large latent heat release (e.g. Nordeng, 1990; Nielsen, 1997). Latent heat release can contribute to intensification through a range of mechanisms. Theories more commonly used to explain hurricane growth, in particular conditional instability of the second kind (CISK) (e.g. Rasmussen, 1979) and wind-induced surface heat exchange (WISHE) (e.g. Emanuel and Rotunno, 1989), have been used to explain the intensification of intensely convective polar lows. Other polar lows possess a similar structure to extratropical cyclones with very strong latent heat release, where an upper-level PV anomaly interacts with a low-level diabatically-produced PV anomaly (e.g. Bresch *et al.*, 1997; Claud *et al.*, 2004). Such structural characteristics can be related to the theoretical work of Snyder and Lindzen (1991), who showed that latent heat release can theoretically act as a 'dynamical surrogate' to basic-state PV gradients at the surface and tropopause.

The CISK and WISHE theories as applied to polar lows both describe a positive feedback loop where a cyclone induces localised tropospheric heating associated with strong convection, which results in further intensification of the cyclone. The theories differ in their closure relating the intensity of the cyclone to the strength of the heating. The formulation of CISK that has been applied to polar lows by Rasmussen (1979) requires an atmosphere that is conditionally unstable (with large convective available potential energy (CAPE)). WISHE on the other hand relates the tropospheric heating directly to fluxes of heat and moisture from the ocean to the atmosphere in an atmosphere that is nearly neutral to moist convection (i.e. small CAPE) (Emanuel, 1986).

The intensification of extratropical cyclones with strong latent heat release has been assessed more

*Correspondence to: Thomas J. Bracegirdle, British Antarctic Survey, Cambridge, CB3 0ET, UK E-mail: tjbra@bas.ac.uk

comprehensively than for polar lows due to the greater ease with which extratropical cyclones can be modelled numerically (due to their larger size) and verified by observations (e.g. Kuo *et al.*, 1991; Stoelinga, 1996; Huo *et al.*, 1999; Ahmadi-Givi *et al.*, 2004). A systematic observational and modelling study of North Atlantic cyclones, FASTEX (Fronts and Atlantic Storm-Track EXperiment, see Joly *et al.*, 1997), provided the basis for the suggestion of a new conceptual model for the life cycle of extratropical cyclones with strong latent heat release: type C cyclogenesis (Deveson *et al.*, 2002; Plant *et al.*, 2003). Type C cyclogenesis is an extension to the type A and B cyclogenesis categories of Petterssen and Smebye (1971). Two type C cyclones that underwent significant development, both FASTEX cases, have been studied in detail (Plant *et al.*, 2003; Ahmadi-Givi *et al.*, 2004). These type C cyclones both possessed large forcing by a pre-existing upper-level trough (characteristic of type B), exhibited a phase tilt between upper and lower levels that did not decrease during intensification (characteristic of type A), and possessed weak baroclinicity in the lower troposphere. Latent heat release was found both to enhance the cyclonic circulation at low levels and to maintain the phase tilt through retardation of the upper-level PV anomaly (Plant *et al.*, 2003; Ahmadi-Givi *et al.*, 2004). A more detailed introduction to type C cyclogenesis can be found in Bracegirdle and Gray (2008).

Recently Bracegirdle and Gray (2008) estimated that approximately one third of polar lows in the Nordic seas are type C cyclones. This estimate was based on quasi-geostrophic (q-g) diagnostics of vertical motion that were developed by Deveson *et al.* (2002). Fundamental to the method of Deveson *et al.* (2002) is the use of the q-g diagnostics to quantify the contributions to mid-tropospheric vertical motion from forcing at upper levels (U) and lower levels (L). The method uses a cyclone lifetime average U/L ratio (averaged over the intensification period) and the evolution of a tilt-like diagnostic of the vertical structure of the cyclone to classify cyclones as type A, B or C. The lifetime average U/L ratio is used to distinguish between the strongly upper-level forced type B and C cyclones and the dominantly lower-level forced type A cyclones. In an analysis of a climatology of extratropical cyclones, Gray and Dacre (2006) found that a lifetime average U/L ratio of greater than 4.0 is characteristic of type C cyclones, less than 2.0 is characteristic of type A and between 2.0 and 4.0 is characteristic of type B. The large U/L ratio in type C cyclones occurs because the q-g diagnostic method used does not include a diabatic heating term, which if included would contribute significantly to L in association with the strong lower-tropospheric latent heat release that is characteristic of developing type C cyclones. This limitation means that this diagnostic cannot cleanly differentiate between weak transient systems forced almost entirely by upper-level processes (i.e. with weak diabatic forcing) and true type C cyclones (Plant *et al.*, 2003).

Plant *et al.* (2003) and Ahmadi-Givi *et al.* (2004) found that the use of PV diagnostics that take explicit account of the role of latent heat release could provide a more complete description of type C cyclogenesis in extratropical cyclones. Therefore as a first step towards a more reliable assessment of type C cyclogenesis in polar lows, we have assessed a polar low using the static piecewise PV inversion approach of Plant *et al.* (2003). As well as elucidating the relative importance and interactions between different processes in the intensification of polar lows, the use of this method provided the possibility for further development of the concept of type C cyclogenesis by adding to the two FASTEX cases that have been studied in detail.

This PL has already been studied previously by Nielsen (1997) and Claud *et al.* (2004). There are three key reasons for returning to this case for further analysis. Firstly, Claud *et al.* (2004) noted the presence of a distinct upper-level PV anomaly, phase locked with the surface cyclone. This, allied with the crucial importance of latent heat release, is characteristic of type C cyclogenesis. In this study we quantify the interaction between different PV anomalies to assess the possible role of type C cyclogenesis. Secondly, the PV diagnostics are used to assess the role of WISHE, which Nielsen (1997) suggested might become important at later stages of the PL life cycle. Thirdly, and more practically, both Nielsen (1997) and Claud *et al.* (2004) successfully simulated the structure and evolution of this case using different numerical models.

The two specific questions addressed in this paper are: (1) To what extent is the life cycle of the PL consistent with type C cyclogenesis according to the criteria of Plant *et al.* (2003) and Deveson *et al.* (2002)? and (2) What is the role of WISHE in the intensification of the PL? In section 2 the model and diagnostic methods are described. The evolution of the PL and an assessment of the model simulation are described in section 3. The results are presented in section 4. Finally, a discussion and answers to the above questions are presented in section 5.

2. Methodology

The method used in this study was to run a numerical weather prediction model simulation of the polar low that occurred on 13 October 1993 and perform PV diagnostics on the model output. Here the details of the numerical model and PV inversion technique are described.

2.1. Numerical model

The UK Met Office Unified Model version 5.5, run on a limited area mesoscale domain, was used for numerical simulations in this study. A general description of the model can be found in Cullen (1993). The current non-hydrostatic dynamical core of the model is detailed in Davies *et al.* (2005). The configuration used in this case is based on the standard forecasting mode, but without data assimilation. The model grid was set up on a rotated latitude/longitude grid with a computational north pole at 24°N, 180°E. Model integrations were

DOI: 10.1002/qj

run with a horizontal grid spacing of 0.11° in both latitude and longitude, which on the rotated grid equates to a horizontal grid spacing over the Nordic seas of approximately 12 km in both latitude and longitude. The limited area domain used has 240 by 260 grid points centred at 66°N, 0°W on the rotated grid. The domain extends between approximately 50°N and 75°N in latitude and 45°W and 45°E (20°W and 20°E) in longitude to the north (south) of the domain. In the vertical the model has 38 levels, with a variable vertical spacing providing the highest resolution (13 levels) in the boundary layer. Version 4A of the Met Office convection scheme was used, detailed in Gregory and Innes (2005). The sea-surface temperature (SST) and sea ice are prescribed and fixed throughout the run. The model simulations were initialised from the European Centre for Medium-Range Weather Forecasts (ECMWF) ERA-40 reanalysis data at 1200 GMT 13 October 1993. The lateral boundary conditions for the duration of each run were provided every six hours by a separate forecast run of the global version of the Met Office Unified Model.

2.2. PV inversion

According to the invertibility principle for balanced motion, a given distribution of PV can be inverted to deduce the wind, temperature and pressure fields (Hoskins *et al.*, 1985). The inversion of a PV field requires the following information to be specified:

- a balance condition,
- the definition of some boundary conditions in order to take account of the global distribution of PV,
- and, if dealing with the anomaly problem, a reference state from which to define anomalous PV.

The PV inversion methodology consists of performing two inversions to quantify the instantaneous wind and temperature distribution attributable to a PV anomaly of interest. One inversion is performed on the full PV field and one on the PV field with the anomaly removed. The difference between the unmodified and modified inverted fields then yields a measure of the contribution of the anomaly to the flow and its interaction with other anomalies. To isolate the PV anomalies associated with the polar low, inversions were conducted on smaller horizontal domains than the mesoscale model domain. The size of the inversion domains was typically 100 by 100 grid points (approximately 1200 by 1200 km).

2.2.1. Balance condition and boundary conditions

The PV inversion method used in this study is based on Davis and Emanuel (1991) and developed and implemented by Ziemianski (1994), Demirtas and Thorpe (1999), Griffiths *et al.* (2000), Pomroy and Thorpe (2000), Plant *et al.*(2003) and Ahmadi-Givi *et al.* (2004). The nonlinear balance condition of Charney (1955) is used in this method. The main assumption of this condition is that the divergent part of the flow is small compared to the rotational part. For most cyclones this condition is satisfied. However, large departures can occur in regions of large divergence associated with strong diabatic heating (Ahmadi-Givi *et al.*, 2004). It was found that for the PL, divergence was an important contributor to the flow at some stages of intensification and therefore the implications of this are considered in the results section (section 4). A caveat of the nonlinear balance approach is that the linear addition of PV anomalies, which is applicable under the assumption of quasi-geostrophic balance, does not strictly apply. However, Birkett and Thorpe (1997) showed that for non-overlapping anomalies, errors due to this effect are tolerably small. For boundary conditions we follow Davis and Emanuel (1991), Ahmadi-Givi *et al.* (2004) and others, where geopotential and stream function are prescribed on the lateral boundaries and their vertical derivatives are specified from potential temperature on the horizontal (top and bottom) boundaries. The PV inversion domain was restricted to the range 850–100 hPa in the vertical to avoid numerical problems in the boundary layer.

A key constraint on the inversion method is that PV must be positive throughout the inversion domain to avoid potentially non-unique or non-converging solutions due to the inversion of negative PV. For the PL, absolute values of PV in regions of negative anomalies were small but there was negligible negative PV. Since the attribution method involves two inversions, one on the full PV field and one with anomalies replaced with reference-state values, inversions of negative anomalies did not require inversions of negative absolute values of PV.

2.2.2. Anomalous PV

The structure of cyclones is often conceptualised in terms of three types of anomalous PV (Davis and Emanuel, 1991; Huo *et al.*, 1999; Plant *et al.*, 2003; Ahmadi-Givi *et al.*, 2004). These consist of upper-level PV (UPV) anomalies, considered to be of stratospheric origin, lower-tropospheric PV (LPV) anomalies, generated by diabatic effects, and surface potential temperature (θ_B) anomalies, which can be viewed as a thin layer of PV at the surface. Ahmadi-Givi *et al.* (2004) found that strong latent heat release in a cyclone produced a negative UPV anomaly in addition to a positive LPV anomaly. Since diabatic effects can reduce PV at upper levels, some authors (Pomroy and Thorpe, 2000; Ahmadi-Givi *et al.*, 2004) have distinguished this reduced upper-level PV (RUPV) from upper-level anomalous PV of stratospheric origin (UPV). Here we do not make this distinction and refer to all anomalous PV at upper levels as UPV whilst recognising that latent heat release may contribute significantly to negative PV anomalies at upper levels. The appropriate method for defining a reference state from which to define anomalies depends on the spatial and temporal characteristics of the type of anomaly being considered.

UPV anomalies generally occur near the tropopause (around 400–300 hPa at midlatitudes). Occasionally intrusions or folds of stratospheric air can penetrate down to around 700 hPa (Cox *et al.*, 1997). High PV air of low

DOI: 10.1002/qj

humidity, associated with a tropopause fold, penetrated down to 650 hPa in the simulated PL. Since the LPV anomaly was always lower than 650 hPa, all PV anomalies at or above 650 hPa were considered as UPV anomalies. UPV anomalies often occur on a background of large horizontal PV gradients associated with the slow-moving background flow in the upper troposphere. In such cases a temporal average is often used to define the reference state, since a spatial average over the region of interest would not capture the background gradients. Various averaging periods have been chosen in previous studies, ranging from five days (Davis and Emanuel, 1991; Stoelinga, 1996; Plant *et al.*, 2003) to two days (Ahmadi-Givi *et al.*, 2004). Ahmadi-Givi *et al.* (2004) found that averaging periods of more than two days smoothed out large-scale structures as well as the local anomaly of interest. Similarly, for the PL a two-day averaging period was found to be appropriate. Distinct positive and negative UPV anomalies were evident during most of the PL lifetime. Both were included in the analysis except for section 4.3 where, for comparison with previous work, the results shown exclude the negative UPV anomaly. In this case the modified PV field was set up with reference-state values in the region of the positive anomaly only.

LPV anomalies are usually easily identifiable as distinct features in the lower troposphere. For defining the reference state a spatial averaging technique is preferred by Plant *et al.* (2003) and Ahmadi-Givi *et al.* (2004), since background PV gradients tend to be weak and a spatial average is more straightforward to calculate than a temporal average. For the same reason, spatial averaging was used to define the LPV anomaly in the PL. For most of the evolution of the PL a distinct positive LPV anomaly was evident, with negligible negative anomalies at all times.

Anomalies in θ_B are defined on the 850 hPa level to avoid issues associated with the planetary boundary layer such as unstable lapse rates. A temporal average was used to define the reference state since strong background temperature gradients were present during the PL life cycle (analogous to the strong PV gradients found at upper levels). A two-day average was found to be suitable for isolating the mesoscale positive θ_B anomaly associated with the PL throughout the simulation. At early times this positive anomaly was embedded within a synoptic-scale negative anomaly, which weakened to become insignificant 24 hours into the PL simulation. This synoptic-scale negative anomaly was associated with a large region of cold advection to the west of a synoptic low and was not filtered out with two (or even one) day temporal averages used as the reference state. This negative anomaly was omitted from the PV diagnostics due to its large scale and brief existence early in the simulation; other negative θ_B anomalies were negligible.

3. Observed and simulated evolution

The intensification phase of the PL lasted for around two days, which is significantly longer than the typical polar low lifetime of around 12–15 hours that was observed by Wilhelmsen (1985). In most cases polar lows are quickly advected over land and subsequently decay. The PL initially formed along a low-level baroclinic zone in the Barents Sea, moved down the Norwegian Sea and decayed over south-western Norway. The small-scale structure of the PL was embedded within a large-scale cold-air outbreak associated with a synoptic low over Scandinavia and high pressure over Greenland. As the PL developed, it moved away from the synoptic low, which remained quasi-stationary over north-eastern Scandinavia (see Figure 2 of Claud *et al.*, 2004).

The cloud structure, as viewed from infrared satellite imagery, changed significantly during the PL's lifetime (Figure 1). The initial formation took place between Norway and Svalbard in a region of enhanced cloudiness along the baroclinic zone (marked by an 'X' in Figure 1(a)). A striking comma cloud structure then rapidly formed between 0000 GMT and 1200 GMT on 14 October (Figure 1(b) and (c)). Strong outflow aloft is indicated by the high-altitude cirrus clouds, which appear bright on the infrared satellite imagery. Later, in the mature stage, multiple convective cells embedded in the centre of the low are apparent (Figure 1(d)). The high cirrus clouds seen previously are no longer as prominent. The PL decayed rapidly once it moved over the land surface of south-western Norway at around 1200 GMT on 16 October.

3.1. Track and intensity in observations and model simulations

The simulation of the PL in the UK Met Office numerical weather-prediction model agrees well with observations in terms of intensity, but the position of the simulated PL deviated from the observed track. In the following text the model integration times refer to the number of hours after the initialisation time (1200 GMT 13 October 1993, denoted T + 0). The model-simulated PL intensified from T + 12 through to around T + 42 (Figure 2). Two observation sources used by Claud *et al.* (2004) show similar values for the maximum near-surface wind speed in the vicinity of the maturing PL. Speeds derived from Special Sensor Microwave/Imager (SSM/I) data from 0714 GMT 14 October show values of up to 24 m s^{-1}. A weather ship positioned in the track of the PL (66°N, 2°E) observed two maxima of sustained wind speed, one at T + 36 and the other at T + 45, both 23 m s^{-1}. The maxima were separated by a period of weak winds as the centre of the PL passed over. The maximum 10 m wind speed within a 200 km radius of the surface PL simulated by the Met Office model for 0600 GMT 14 October (T + 42) was also 23 m s^{-1}, in good agreement with the satellite-retrieved and *in situ* data. However, the model-simulated PL made landfall one day earlier than observed at around 1200 GMT 15 October (T + 48). This is due to a position error in the track of the simulated PL, which from a comparison with satellite imagery was estimated to be ∼5° too far to the east and ∼1° too far to the south at T + 42. This might be a consequence of

DOI: 10.1002/qj

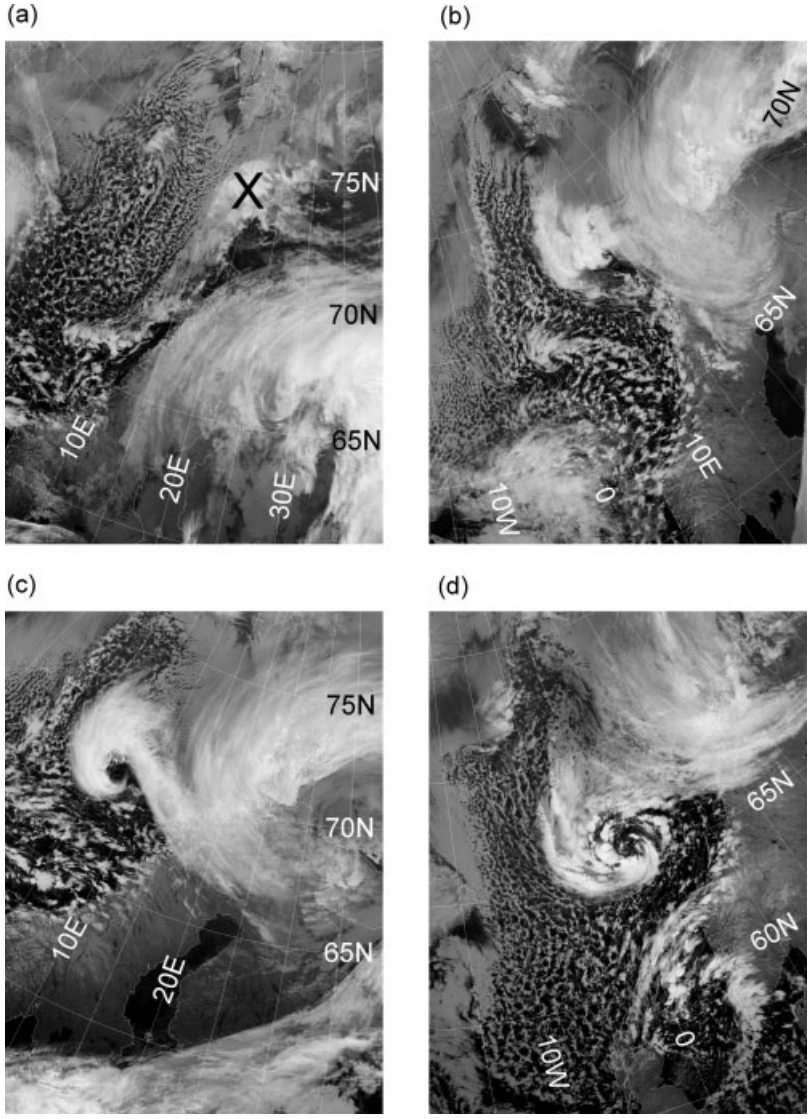

Figure 1. Infrared satellite imagery for (a) 1401 GMT 13 October 1993, (b) 0536 14 October, (c) 1349 14 October and (d) 0524 15 October. NOAA AVHRR imagery retrieved courtesy of the NERC Dundee Satellite Receiving Station. The 'X' in (a) marks the location of the incipient polar low at the surface.

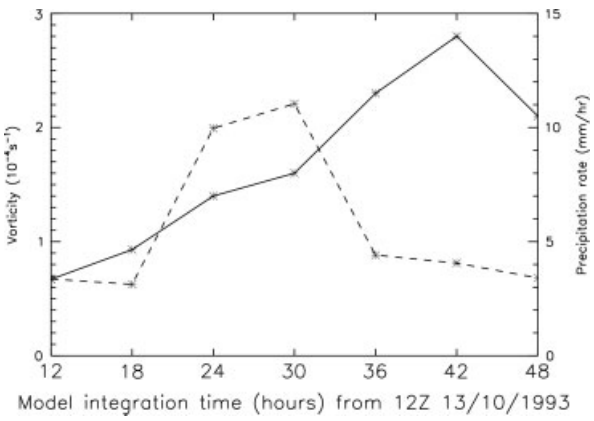

Figure 2. The solid line shows the vertical component of relative vorticity at 900 hPa averaged over an area of 150 km radius from the surface pressure minimum (scale on left axis). The dashed line shows the maximum precipitation rate (units of mm h^{-1}) within a 150 km radius of the surface pressure minimum (scale on right axis). Data are from model output and plotted at six-hour intervals.

the low resolution of the initial conditions provided by ERA-40 since a position error is already evident early in the PL simulation. For instance at T + 24 it was estimated from satellite imagery that the simulated PL is positioned ~3° too far to the east and ~0.5° too far to the south.

Claud *et al.* (2004) simulated the PL with two different versions of the same Norwegian Limited Area Model. One version (NORLAMS) simulated the PL 4° too far west and 0.5° too far north by T + 48 (1200 GMT 15 October). However, the other version, with more vertical levels in the boundary layer and a different cloud parametrization scheme (NORLAM) produced a track that closely matched observations.

Observations reported by Claud *et al.* (2004) indicate that the main intensification phase had ended by T + 48. Therefore the Met Office model simulation captures the intensification phase before the simulated PL makes landfall, but not the maintenance and decay phase. We therefore focus on the intensification phase of the PL.

DOI: 10.1002/qj

3.2. Simulated PV structure and evolution

The simulated evolution of the UPV structure as seen on the 285 K isentropic surface is shown in Figure 3. This corresponds to around 450 hPa, which is the approximate height of the tropopause in this case. In the absence of frictional and diabatic effects, air parcels will flow along constant potential temperature surfaces and the isentropic PV of a given air parcel is conserved. Thus the maps shown in Figure 3 show a surface on which PV may be considered as a tracer of the atmospheric flow. Any alterations to the PV following the flow on this surface will be due to non-conservative effects such as diabatic heating. At the genesis stage of the polar low (T + 12) there is a region of high PV values situated at ~74°N and between 0° and 10°E (Figure 3(a)). This region of anomalously high PV values is due to the dry intrusion associated with the synoptic low situated over northern Scandinavia. As this moves to the south at later times the effects of the intensifying PL become apparent. By T + 24 the comma cloud structure of the PL is evident as a region of low PV values (cf. Figures 1(c) and 3(b)). The region of high PV values is stretched to form a thin PV streamer that encircles the south and west of the surface PL by T + 42 (Figure 3(c)). By T + 42 the region of anomalously low PV values dominates the upper troposphere above the surface PL.

The simulated evolutions of LPV and θ_B are shown in Figure 4. In Figure 4 θ at 850 hPa is overlaid with the LPV (the average PV in the lower troposphere, between 850 and 650 hPa). Between T + 6 and T + 12 a shallow

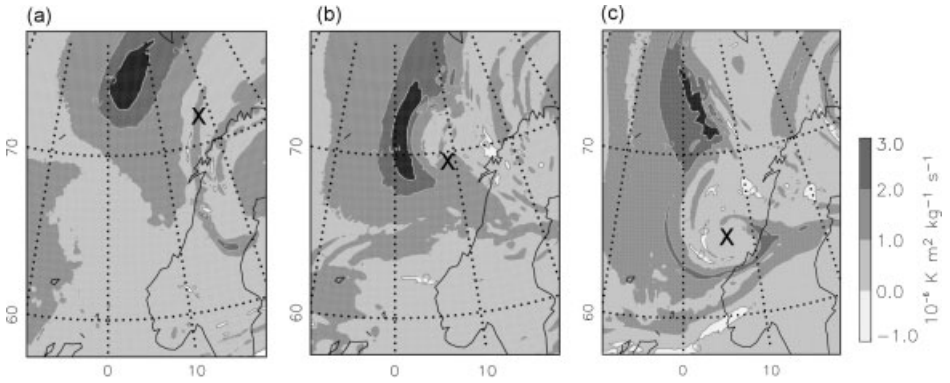

Figure 3. PV on $\theta = 285$ K for (a) T + 12, (b) T + 24 and (c) T + 42. The contour intervals are 1 PV unit (PVU), where 1 PV unit is equivalent to SI units 1×10^{-6} m^2 s^{-1} K kg^{-1}. The 'X' in each panel indicates the location of the minimum of the 1000 hPa geopotential height.

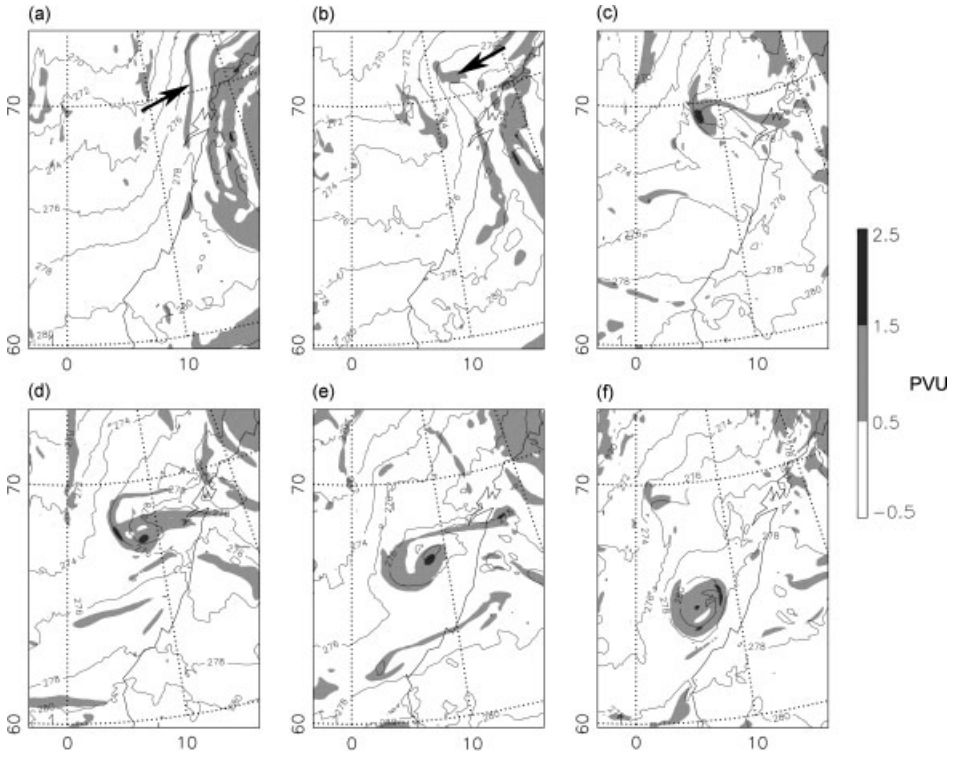

Figure 4. 850 hPa potential temperature (contours at intervals of 2 K) and lower-tropospheric interior PV averaged between 850 hPa and 650 hPa (shading from 0.5 PVU upwards at intervals of 1 PVU) for (a) T + 12, (b) T + 18, (c) T + 24, (d) T + 30, (e) T + 36 and (f) T + 42. The arrow in (a) indicates a shallow band of PV and the arrow in (b) shows the location of the incipient surface polar low.

DOI: 10.1002/qj

band of anomalous LPV (up to 800 hPa) forms adjacent to the Norwegian coast, marked by the arrow in Figure 4(a). An indication that latent heating generated this PV is the presence of a band of precipitation produced by the model in the same location (not shown). A collocated band of cloud can also be seen in satellite imagery (Figure 1(a)) and there is a collocated UPV anomaly (Figure 3(a)). Increased precipitation within the warm anomaly coincides with a stronger patch of LPV at the centre of the surface warm anomaly by T + 18, with vertically averaged values exceeding 1 PV unit (PVU: equivalent to SI units 1×10^{-6} m^2 s^{-1} K kg^{-1}) (the LPV maximum is indicated by the arrow in Figure 4(b)). The surface warm anomaly amplifies over the same period. The model-simulated structure is consistent with the infrared satellite imagery, which shows a small-scale patch of cloud in a comma shape embedded within the warm anomaly (Figure 1(b)). It seems likely that the main trigger was dynamically forced ascent, since according to the model there was not much CAPE (not shown). A rapid increase of the LPV then occurs between T + 18 and T + 24 (Figure 4(b) and (c)). This increase is collocated with an increasing horizontal temperature gradient and a large surface precipitation rate (Figure 2 and Figure 5(b)). The precipitation at this stage is mainly classified as 'large scale' by the model, indicating forced ascent associated with frontogenesis. During the following 12 hours, up to T + 36, PV continues to be formed in a region of precipitation on the western flank of the polar low as the surface warm anomaly secludes (Figure 4(d) and (e)). The precipitation produced by the model during this period changes from large-scale to convective (implying generation by the convective parametrization scheme) and reduces in intensity (Figure 2). Continued strong fluxes of sensible and latent heat from the ocean to the atmosphere over this period maintain active convection.

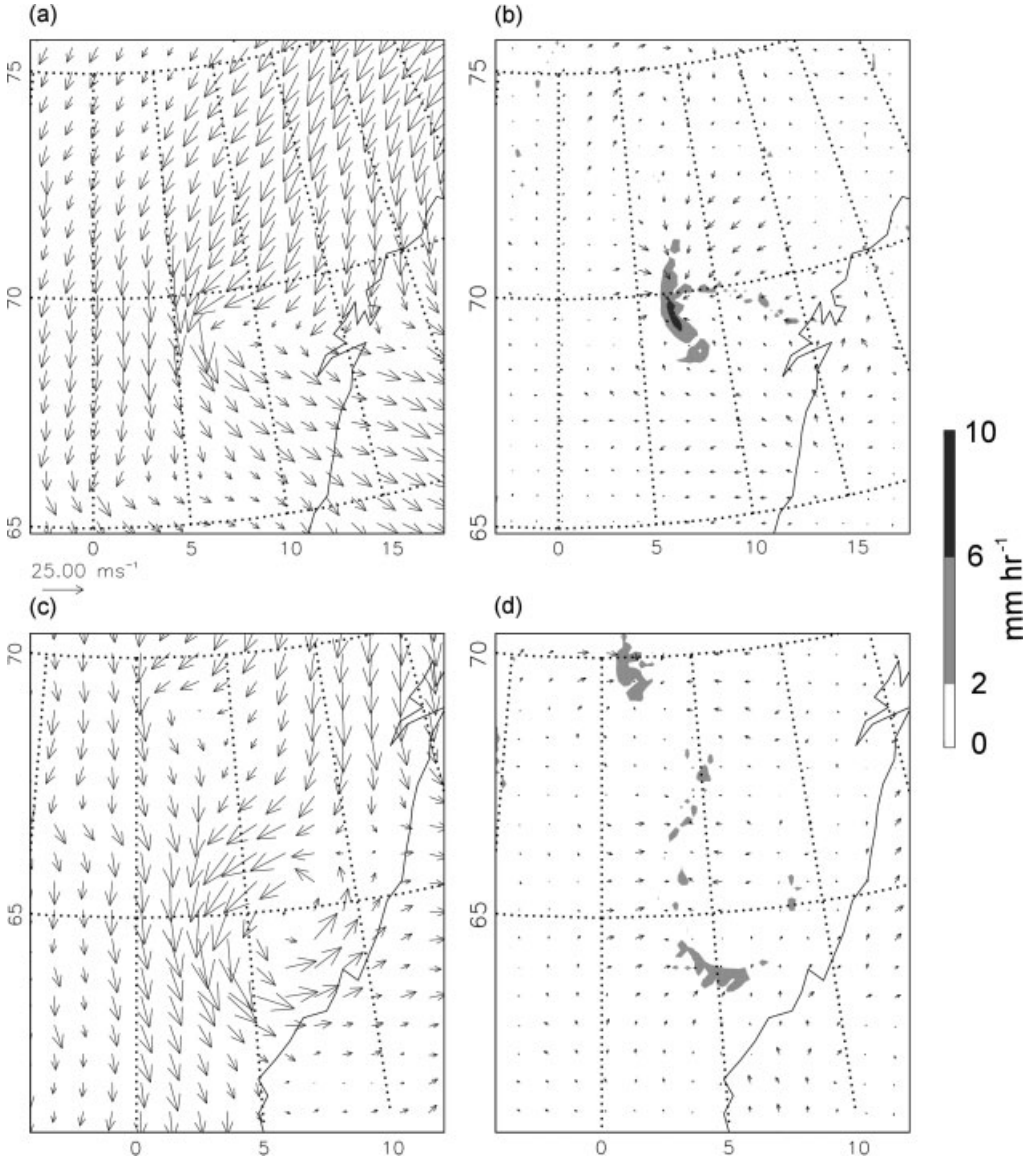

Figure 5. Wind vectors of the full winds directly from the model (a), (c) and the full minus the inverted winds (b), (d) at 850 hPa and T + 24 (a), (b) and T + 42 (c), (d). The precipitation rate is also shown for T + 24 (b) and T + 42 (d). The scale of the wind vectors is indicated to the left of the plots and the grey-scale shading for the precipitation rate is to the right.

DOI: 10.1002/qj

Model-estimated total heat fluxes of up to ~700 W m^{-2} were found (not shown), which is similar in magnitude to the fluxes associated with category one hurricanes (Miner *et al.*, 2000). At T + 42 (Figure 4(f)) large LPV values encircle much of the warm anomaly and the period of rapid intensification has ended. The time taken for the LPV formed at T + 24 to wrap up is around 18 hours, which is consistent with what one would expect from the properties of the PL (i.e. a motion-relative wind speed of ~12 m s^{-1} at a radius of ~100 km).

4. Piecewise PV inversion results

4.1. The importance of the divergent part of the flow

The balance condition on which the PV inversion technique is based assumes that the divergent part of the wind is small compared to the rotational part (see section 2.2). To assess the accuracy of the PV inversion technique, the wind resulting from the inversion of the unmodified PV field ($\mathbf{V}_{inv}$) was compared to the full model horizontal wind field ($\mathbf{V}_{full}$). At most locations and times, departures from balance (the magnitude of $\mathbf{V}_{full} - \mathbf{V}_{inv}$ compared to the magnitude of $\mathbf{V}_{full}$) were found to be small. In the vicinity of the surface PL at 850 hPa (taken here as a spatial average within a radius of 100 km from the sea-level pressure minimum), the departures from balance were found to be 10–15% at T + 12, T + 18, T + 36, T + 42 and T + 48, and were ~25% for T + 24 and T + 30. This indicates that the main features of the flow are captured by the inversion method for most times. However, at T + 24 and T + 30 strong convergence is collocated with regions of strong diabatic heating (inferred here from the precipitation rate since a diagnostic of diabatic heating was not available, Figure 2 and Figure 5(a) and (b)). A reduction of the maximum precipitation rate at later times coincides with smaller departures from balance (Figure 2 and Figure 5(c) and (d)). The infrared satellite imagery is consistent with the reduction of the importance of the divergent part of the flow as the PL approached its mature stage. Widespread cirrus outflow was present during rapid development (Figure 1(c)) and subsequently reduced in extent (Figure 1(d)).

The reasonable accuracy of the inverted flow at the mature stage of the PL indicates that divergence at earlier times can mainly be attributed to latent heat release. The relatively large magnitude of the divergent flow at T + 24 and T + 30 shows that its effect must be taken into account when assessing interactions between different PV anomalies.

4.2. The interaction between PV anomalies

The horizontal wind attributable to a given anomaly type may increase or decrease the amplitude and/or change the location of neighbouring anomalies. During the genesis stage of the PL (T + 12) the wind field induced by a positive UPV anomaly dominates the surface flow over negligible effects from the LPV and θ_B anomalies

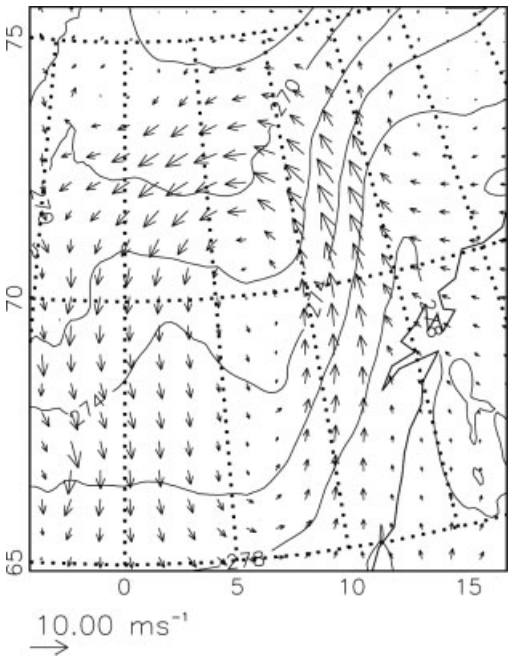

Figure 6. Contours of 850 hPa potential temperature (contour interval 2 K) overlaid with arrows of 850 hPa winds attributable to anomalous UPV at T + 12.

(Figure 6). The near-surface winds induced by anomalous UPV contribute to warm advection in the region of the developing warm anomaly at around 72°N and 12°E.

The near-surface (850 hPa) flow attributable to different anomaly types during the rapid intensification period (T + 30) is shown in Figure 7. This provides information on the role of the different PV anomaly types in the evolution of θ_B anomalies. The inverted flow at 850 hPa is dominated by that attributable to the positive LPV anomaly, which induces warm advection northwest of its centre and cold advection to its southeast acting to seclude the surface warm anomaly (Figure 7(a)). Near-surface winds attributable to anomalous UPV are weaker, but show a clear combined effect of the positive and negative UPV anomalies, which act to amplify the positive θ_B anomaly (Figure 7(b)). The self-interaction of the θ_B anomaly shows a contribution to the subsequent warm air seclusion at the surface (Figure 7(c)). Low-level convergence is induced by diabatic heating in the region of strong latent heat release to the northwest of the surface PL (Figure 7(d)). Although the accuracy of the PV diagnostics is strongly affected by latent heat release to the northwest of the centre of the PL, it is clear that the winds attributable to the LPV anomaly dominate the low-level wind field.

The upper-level (450 hPa) flow attributable to different anomaly types during rapid intensification is shown in Figure 8. This provides information on the role of the different PV anomaly types in the evolution of UPV anomalies. The evolution of the anomalous UPV at T + 30 is strongly influenced by the diabatically induced divergent flow at 450 hPa (Figure 8(d)). In particular the divergent winds act to advect the positive UPV anomaly towards the south and west. The self-interaction of anomalous UPV

DOI: 10.1002/qj

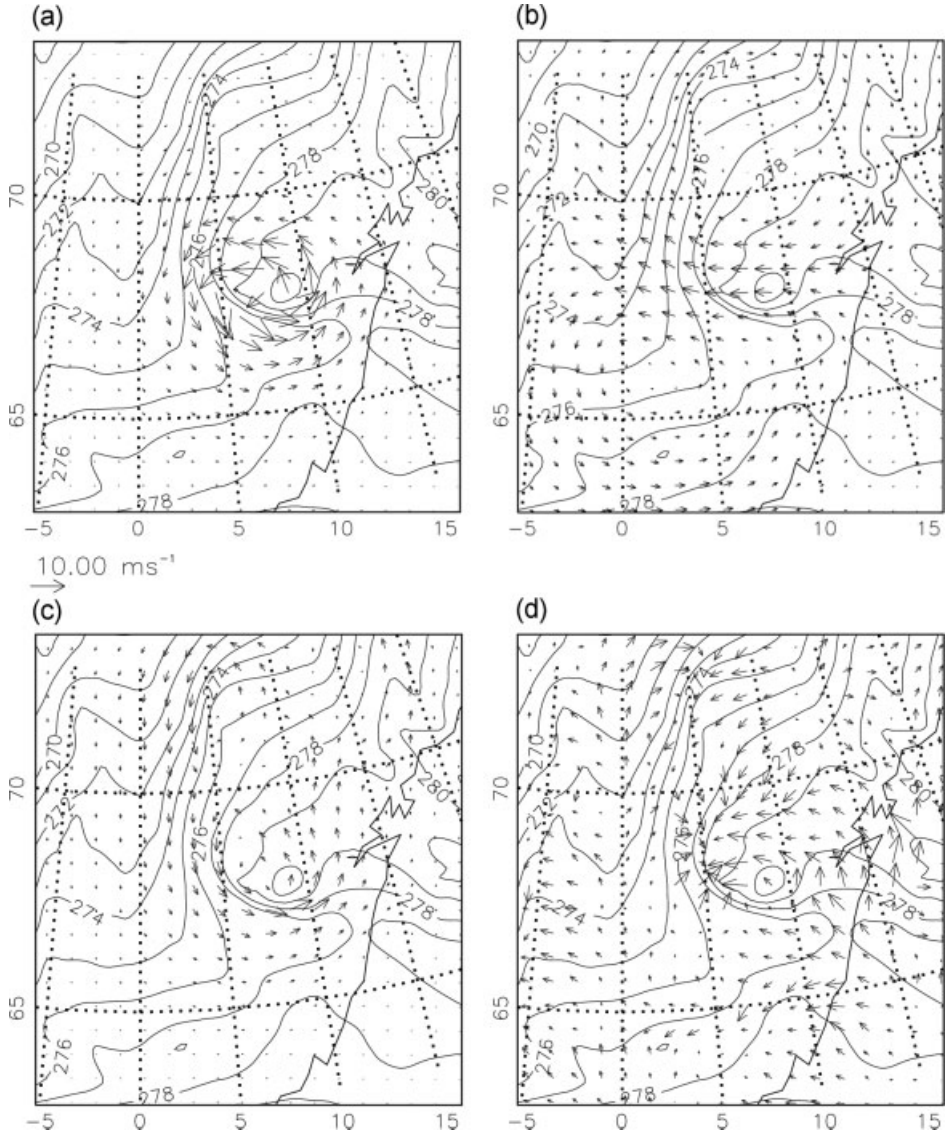

Figure 7. Contours of 850 hPa potential temperature at T + 30 (contour interval 1 K) overlaid with arrows of 850 hPa wind attributable to (a) anomalous LPV, (b) anomalous UPV, (c) θ_B anomalies and (d) the difference between the full wind directly from the model and the wind inverted from the unmodified PV field.

acts to induce southward propagation of the upper-level anomaly structure (Figure 8(b)). The winds attributable to the LPV anomaly act to amplify both the positive and negative UPV anomalies through advection of the upper-level PV gradient, but are relatively weak (Figure 8(a)). The effect of the θ_B anomaly on anomalous UPV is negligible (Figure 8(c)).

A key implication of the strong upper-level divergence is that there are large errors in the upper-level attributed winds. One robust result is the weak winds attributable to the θ_B anomaly, since the amplitude of both the θ_B anomaly itself and its attributed effect do not change substantially as the rate of latent heat release subsides from T + 30 to T + 36.

As the PL approaches maturity at later times (T + 36 onwards) the negative UPV anomaly strengthens and the attributed wind field dominates contributions from UPV over a weakening positive anomaly (not shown). However, as will be seen in the next section, the winds induced by the LPV anomaly continue to dominate the near-surface circulation.

4.3. Relative contribution of different PV anomalies

A diagnostic used by Plant *et al.* (2003) and Ahmadi-Givi *et al.* (2004) to distinguish type C cyclogenesis is the relative contribution of different types of anomalous PV to the surface cyclone depression. They quantify the contribution of a given anomaly type as the maximum geopotential height perturbation in the 850 hPa geopotential height field attributable to that anomaly. Their method does not take into account negative anomalies, but this was not found to be qualitatively important to the analysis of the PL (see appendix).

The evolution of the contribution from different anomaly types is shown in bold in Figure 9. Calculations with the negative UPV anomaly included are shown by the faint dashed line (see appendix). Inversions were

DOI: 10.1002/qj

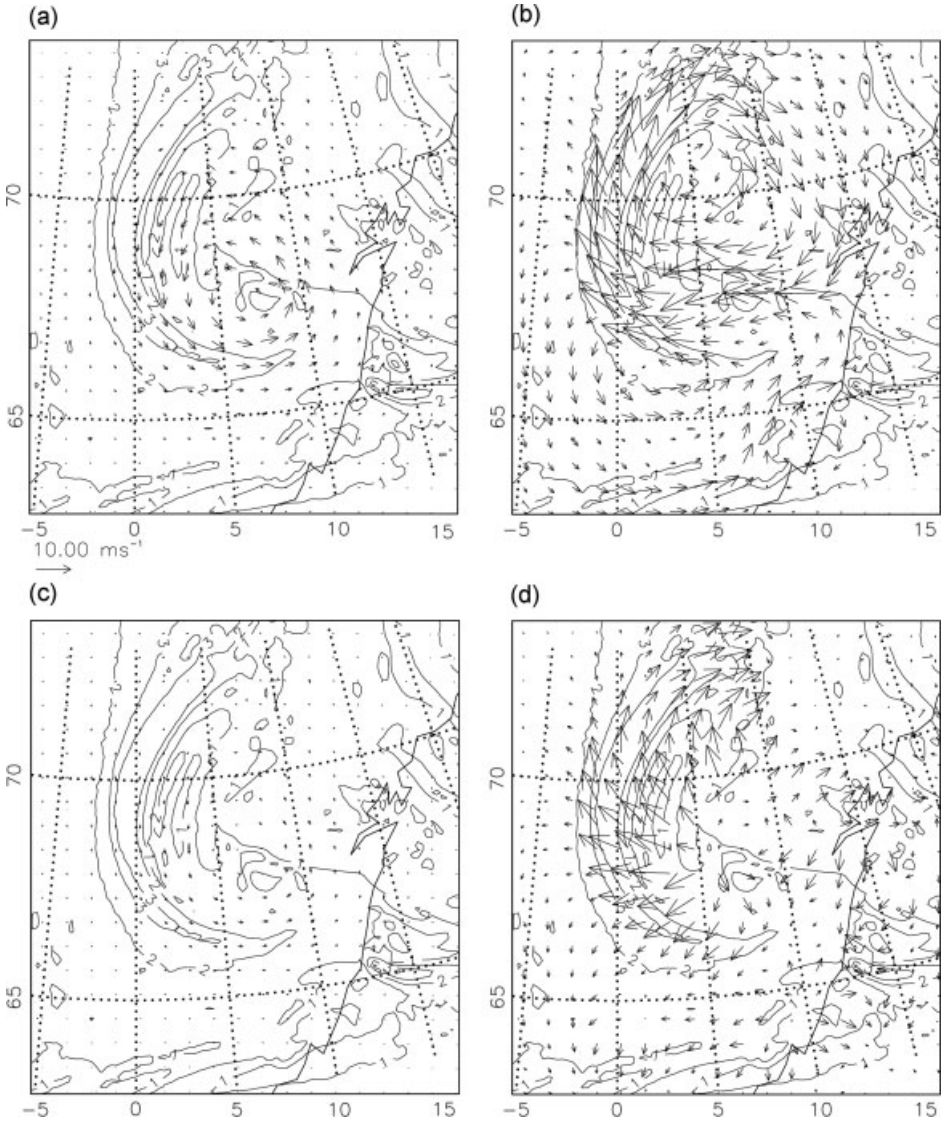

Figure 8. Contours of PV at 450 hPa at T + 30 (contour interval 1 PVU) overlaid with arrows of 450 hPa winds attributable to (a) anomalous LPV, (b) anomalous UPV, (c) θ_B anomalies and (d) the difference between the full wind directly from the model and the wind inverted from the unmodified PV field.

performed on data output at six-hourly intervals through the simulated PL from T + 12 to T + 48. At the genesis stage of development (T + 12) the UPV anomaly was found to be the main contributor, with negligible contributions from both the LPV and θ_B anomalies. Between T + 12 and T + 24, contributions from both the θ_B and LPV anomalies increase at a similar rate to reach the same value as the contribution from the UPV anomaly at T + 24. After T + 24 the contribution from the LPV anomaly increases further to a maximum value at T + 42. The contributions from the UPV and θ_B anomalies remain approximately constant between T + 24 and T + 42 inclusive. As a result, by T + 42 the contribution from the LPV anomaly is more than double the contributions from each of the other anomalies. The contribution from the θ_B anomaly at T + 48 was difficult to define due to the influence of orography over Norway and therefore has not been included in Figure 9. The dominance of the LPV anomaly in the intensification of the PL is supported by an alternative attribution approach using the quasi-geostrophic (q-g) omega equation (Clough *et al.*, 1996). The results are shown in Bracegirdle (2006).

The results for T + 24 and T + 30 are less reliable than at other times due to strong latent heat release. However, the 850 hPa geopotential height perturbations attributable to the UPV and θ_B anomalies do not seem to be significantly affected, since both the amplitude of the anomalies themselves and the geopotential height perturbations attributed to them do not change substantially as latent heating subsides between T + 30 and T + 36.

4.4. Type C cyclogenesis

Key characteristics of type C cyclogenesis found in the diagnostic studies of two FASTEX type C cyclones (Plant *et al.*, 2003 and Ahmadi-Givi *et al.*, 2004) are: (1) the crucial role of latent heat release to development, (2) the dominant initial role of a UPV anomaly which maintains a phase tilt with the surface cyclone through the retardation

DOI: 10.1002/qj

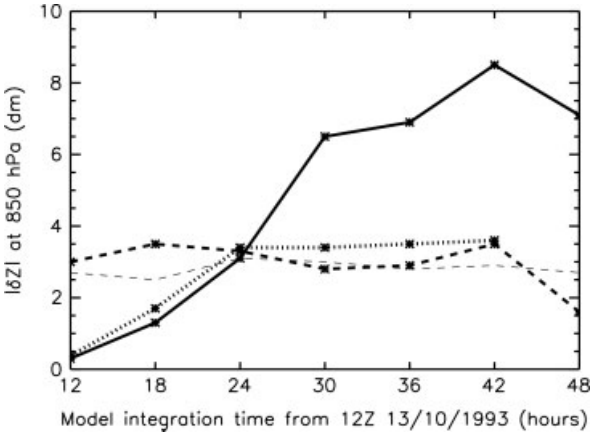

Figure 9. The magnitude of geopotential height perturbations at 850 hPa attributable to anomalous LPV (solid line), anomalous UPV (dashed line) and surface thermal (θ_B) anomalies (dotted line). The thick lines show results from the method used by Plant *et al.* (2003) (for which negative anomalies are omitted). The thin dashed line shows the combined contribution from the positive and negative UPV anomalies. Inversions were calculated at six-hourly intervals.

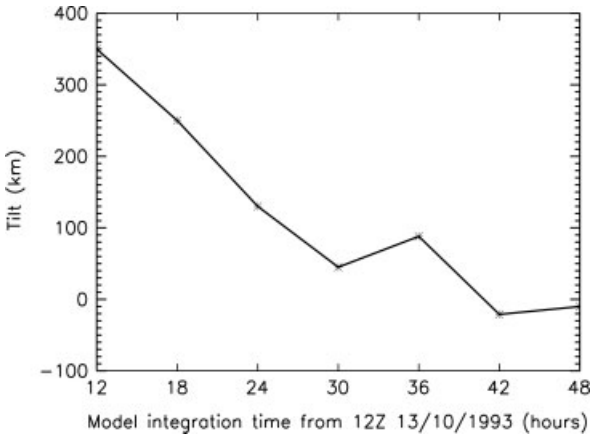

Figure 10. The time evolution of a tilt diagnostic. The distance shown is that between the cyclone surface centre and the maximum in the 850 hPa geopotential perturbation due to the positive UPV anomaly. Distances are calculated in the direction of propagation of the PL. Positive values indicate a tilt leaning away from the direction of the background thermal wind vector (a southward tilt in this case).

of UPV by latent heat release, and (3) the consistently weak influence of a surface thermal (θ_B) anomaly.

The crucial role of latent heat release in the intensification of the PL has previously been established by both Nielsen (1997) and Claud *et al.* (2004). They conducted sensitivity experiments in which the omission of the effects of latent heat release significantly reduced the intensity of numerical simulations of the PL. The prominent role of latent heat release is also evident from the PV diagnostics conducted in this study. The instantaneous 850 hPa geopotential height perturbation attributable to the diabatically generated LPV anomaly was found to be larger than that attributed to the UPV and θ_B anomalies after T + 24 (Figure 9).

The maintenance of a phase tilt during intensification is also an important aspect of type C cyclogenesis. Following Plant *et al.* (2003) we used the distance between the surface low and the maximum 850 hPa geopotential height perturbation attributable to the positive UPV anomaly as a measure of the tilt of the PL. The tilt distance was measured along an axis in the direction of propagation of the PL (whereas Plant *et al.* (2003) used east–west distance due to the north–south elongation of the first system they analysed). Positive values indicate a tilt in the opposite direction to the background thermal wind vector (a southward tilt in this case). According to this tilt diagnostic, the tilt decreased with time to around 50 km by T + 30 (Figure 10). Some tilt was then re-established at T + 36, before decreasing to near zero by T + 42. This tilt evolution is also evident in the horizontal distance between minima in the 1000 hPa and 500 hPa geopotential height fields (not shown) and is consistent with Claud *et al.* (2004), who suggested that the interaction between anomalous UPV and the surface PL ceases after T + 36. The mechanism that results in the short period of increased tilt could be that seen in type C cyclones. Plant *et al.* (2003) suggest that both divergent flow aloft and direct reduction of upper-level PV are potentially important for reducing UPV above regions of latent heat release and maintaining a phase tilt. For the PL the action of upper-level divergence induced by latent heat release is consistent with the changes of the phase tilt through advection of the positive UPV anomaly. The largest divergent flow acting in a southerly direction in the region of the positive UPV anomaly was found to occur at T + 30, after which there was an increase of the phase tilt. The magnitude of the divergent winds at T + 30, nearly double the propagation speed of the surface PL of 5 m s^{-1}, is large enough to explain the increase in the phase tilt by T + 36. A subsequent decrease of divergent flow between T + 36 and T + 42 coincided with a decrease of the phase tilt. However, such evidence is circumstantial; other possible influences such as the direct reduction of upper-level PV by latent heat release could not be quantified and the evidence of an increased tilt is based on a single data point.

The contribution of the θ_B anomalies to the near-surface geopotential height perturbation in the PL is similar in magnitude to the contribution from UPV (Figure 9). In relative terms this is larger than the negligible contribution that has been found in the FASTEX type C cyclones. However, the consistently negligible effect of the θ_B anomaly on anomalous UPV (Figure 8(c)) is consistent with the dynamical characteristics emphasised by Plant *et al.* (2003). It is also possible that some diabatic amplification of the surface thermal anomaly in the PL occurred through the large sensible heat fluxes from the ocean to the atmosphere; this process has not been considered in analyses of midlatitude type C cyclones. Evidence for this can be seen in Figure 4(f) where 850 hPa temperatures within the warm anomaly are higher than the surrounding region, suggesting that local heating as well as advection contributed to the anomaly. In terms of the classification method of Deveson *et al.* (2002), the non-negligible low-level forcing results in a small lifetime average upper- to lower-level q-g forcing (U/L) ratio of 1.1, which varies little from T + 12 to T + 48 (U/L

DOI: 10.1002/qj

was calculated using the same methodology as Deveson *et al.* (2002)). This contrasts with the large U/L ratios ($U/L > 4.0$) found in type C cyclones by Gray and Dacre (2006) and is more typical of type A cyclones. As in Plant *et al.* (2003), this emphasises that PV diagnostics are required for a full description of type C cyclogenesis.

4.5. Role of WISHE

The interaction between the baroclinic dynamics and anomalous LPV between T + 24 and T + 36 means that it is difficult to determine the role of WISHE in the intensification before T + 36. Nielsen (1997) noted that the maximum divergence induced by latent heat release is collocated with the location of maximum surface heat fluxes from T + 24 onwards, consistent with WISHE. However, it is apparent that moisture convergence associated with rapid frontogenesis (Figure 4(b)–(d)) may have added to the heating supplied by surface fluxes. The dynamics are simpler from T + 36. By this time rapid mesoscale frontogenesis has ended and the low-level warm anomaly has secluded to form a warm core. Figure 2 shows that the intensification of the simulated PL after T + 36 contributes 18% relative to its intensity at T + 42 although the proportion of intensification after T + 36 may be significantly larger than this if the maximum intensity is larger than at T + 42 (data were only output at 6-hour intervals). Three points indicate the dominance of WISHE from T + 36: (1) the weak baroclinic interaction between different PV anomalies, (2) small CAPE in the vicinity of the PL (found by Nielsen (1997)), and (3) the large surface heat fluxes (an experiment with surface fluxes turned off at T + 30, not shown, yielded a cyclone that weakened rapidly after this time).

One slight inconsistency with WISHE, found by Nielsen (1997), is that the horizontal size of the PL is slightly larger than the theoretical optimum for the intensification of an axisymmetric vortex. To initiate the intensification of an axisymmetric vortex by WISHE, an initial perturbation must exist that is of a large amplitude and possesses a small radius of maximum near-surface wind (RMW) compared to the local Rossby radius of deformation (*Ro*) (Emanuel and Rotunno, 1989). Assuming that the maximum tropospheric heating is collocated with the RMW, Emanuel and Rotunno (1989) found that an RMW larger than *Ro* leads to the spin-up of an upper-level vortex inside the RMW which will not increase surface fluxes as required by WISHE. Nielsen (1997) found that the RMW was approximately 175 km compared to an *Ro* of 150 km (the stage in development at which these estimates were made was not specified). These conditions are not strongly conducive to intensification by WISHE according to the criteria of Emanuel and Rotunno (1989). However, we found a smaller RMW for the part of the wind field attributable to anomalous LPV, 120 km at T + 36. Our estimate of *Ro* for T + 36 yielded a similar value to that found by Nielsen (1997). Therefore in our simulations, conditions at T + 36 are favourable for intensification of anomalous LPV by WISHE.

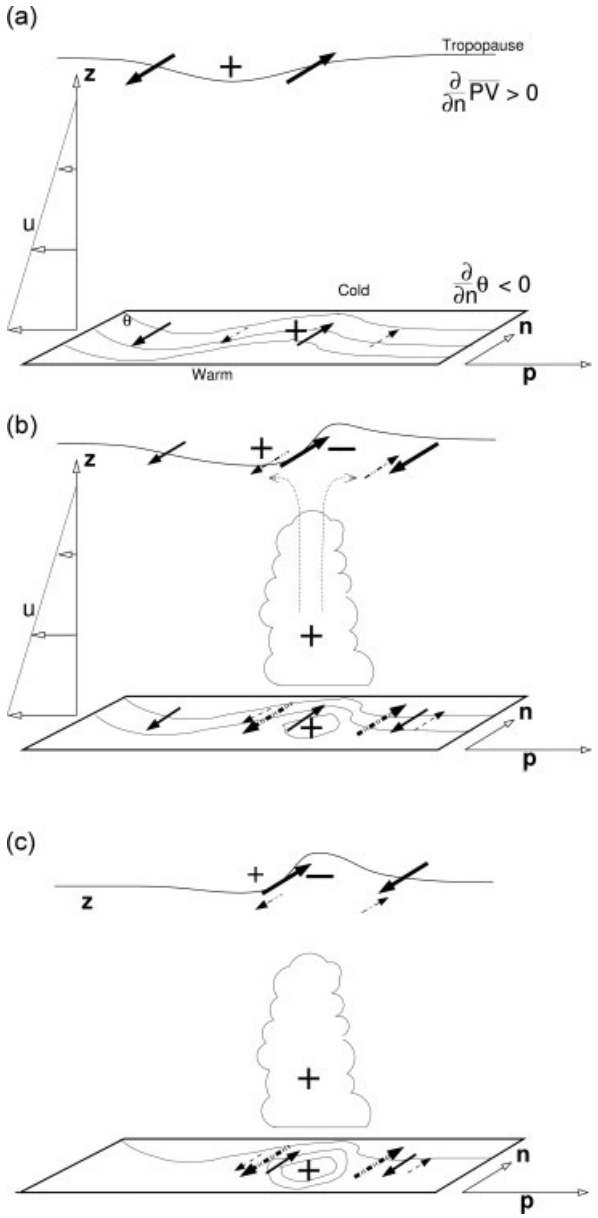

Figure 11. A schematic diagram of the different stages of the intensification of the PL: (a) initial baroclinic stage, (b) baroclinic stage with strong latent heat release, and (c) non-baroclinic WISHE stage. Each category of anomaly (UPV, LPV and surface θ_B) is shown by a '+' symbol for positive anomalies and a '−' symbol for negative anomalies. For clarity, weak effects are not included in the diagram. '**n**' and '**p**' denote unit vectors normal and parallel to the background thermal wind vector respectively (approximately west and north respectively for this PL) and '**u**' is the background flow. '**u**' is not shown in panel (c) since the background wind shear is negligible at this stage. The **n** component of circulations induced by the anomalies are represented by arrows with filled arrow heads and their relative strength is indicated by the thickness and length of the arrows. The induced circulations from the UPV, LPV and θ_B anomalies are shown by solid lines, dash-double-dot lines and dashed lines respectively. The curved dotted arrows collocated with the cloud in panel (b) indicate unbalanced divergent flow associated with strong latent heat release.

5. Discussion and conclusions

The dynamics of an unusually long-lasting polar low that occurred on 13 October 1993 have been investigated with the aid of potential vorticity diagnostics performed on the output from an NWP simulation. The main aims of

DOI: 10.1002/qj

this paper were to determine whether the life cycle of the PL is consistent with a recently proposed category of cyclogenesis, type C (Deveson *et al.*, 2002), and to assess the role of wind-induced surface heat exchange (WISHE) in its intensification.

The intensification of the PL can be split into three stages, shown in Figure 11. This contrasts with previous studies of polar lows in which intensification has been conceptualised in two stages: an initial baroclinic stage with a large adiabatic contribution to the quasi-geostrophic (q-g) vertical motion, followed by a secondary non-baroclinic maintenance stage for which the adiabatic contribution to the q-g vertical motion is relatively weak (e.g. Sundqvist *et al.*, 1989; Nordeng, 1990). For this PL the initial baroclinic phase can be considered to consist of two stages of intensification. The first stage (to T + 24) was dominated by the arrival of an upper-level PV anomaly over a low-level baroclinic zone (Figure 11(a)), whilst the second stage (T + 24 to T + 36) was characterised by strong latent heat release and the maintenance of a vertical tilt of the geopotential height perturbation (Figure 11(b)). A third stage of intensification (T + 36 to T + 42) then occurred as a deep warm core formed (Figure 11(c)).

Stages one and two of the intensification of the PL are consistent with type C cyclogenesis according to the investigations of Plant *et al.* (2003) and Ahmadi-Givi *et al.* (2004). The principal feature is the crucial role of lower-tropospheric latent heat release and the associated maintenance of a phase tilt by retardation of the positive UPV anomaly. One contrast is a non-negligible contribution of the θ_B anomaly to the near-surface geopotential height perturbation, but its weak influence on anomalous UPV is consistent with other type C cyclones. The non-negligible θ_B anomaly results in a small U/L ratio, illustrating that the method of Deveson *et al.* (2002) is not suitable for detecting type C cyclogenesis in the PL. A period of intensification (stage three) during which WISHE seemed to dominate contributed at least 18% to the mature amplitude of the surface PL. During stage two it was difficult to determine the role of WISHE due to strong baroclinic interactions between the LPV and a low-level frontal zone.

Acknowledgements

The authors thank the Met Office for the use of their Unified Model and for the advice and support in using the model provided by the University/Met Office Joint Centre for Mesoscale Meteorology at the University of Reading. We also gratefully acknowledge the use of diagnostic and plotting tools supported by Chang-Gui Wang via the National Centre for Atmospheric Science (NCAS). Robert Plant and Brian Hoskins are thanked for their advice and helpful discussions. Two anonymous reviewers are also thanked for their useful comments. Thomas Bracegirdle was supported by a studentship from the UK Natural Environment Research Council; studentship reference NER/S/A/2002/10539.

Appendix

In section 4.3 the method of Plant *et al.* (2003) and Ahmadi-Givi *et al.* (2004) was used to calculate the relative contribution of different anomaly types to the surface depression of the PL. Their method only takes into account the contribution from positive anomalies. To determine the sensitivity of the results to the inclusion of negative PV anomalies, a further set of calculations were conducted, which included the effects of both positive and negative anomalies. Since the negative anomalies of LPV and θ_B are negligible, the revised calculations were only important for anomalous UPV.

Inversions that included the positive and negative UPV anomalies produced a dipole in the attributable 850 hPa geopotential height perturbation. The contribution from UPV was quantified as the difference between the highest and lowest perturbation values, which is a measure of the dipole strength. This produced very similar values to those calculated from only the positive UPV anomaly (Figure 9), since the inclusion of the negative UPV anomaly dampens the cyclonic perturbation produced from inversion of the positive UPV anomaly alone.

References

Agusti-Panareda A, Thorncroft CD, Craig GC, Gray SL. 2004. The extratropical transition of hurricane Irene (1999): A potential-vorticity perspective. *Q. J. R. Meteorol. Soc.* **130**: 1047–1074.

Ahmadi-Givi F, Craig GC, Plant RS. 2004. The dynamics of a midlatitude cyclone with very strong latent-heat release. *Q. J. R. Meteorol. Soc.* **130**: 295–323.

Birkett HR, Thorpe AJ. 1997. Superposing semi-geostrophic potential-vorticity anomalies. *Q. J. R. Meteorol. Soc.* **123**: 2157–2163.

Bracegirdle TJ. 2006. 'The role of convection in the intensification of polar lows.' PhD thesis, The University of Reading, Reading.

Bracegirdle TJ, Gray SL. 2008. An objective climatology of the dynamical forcing of polar lows in the Nordic seas. *Int. J. Climatol.* **28**: 1903–1919.

Bresch JF, Reed RJ, Albright MD. 1997. A polar-low development over the Bering Sea: Analysis, numerical simulation, and sensitivity experiments. *Mon. Weather Rev.* **125**: 3109–3130.

Charney JG. 1955. The use of the primitive equations of motion in numerical prediction. *Tellus* **7**: 22–26.

Claud C, Heinemann G, Raustein E, McMurdie L. 2004. Polar low le Cygne: Satellite observations and numerical simulations. *Q. J. R. Meteorol. Soc.* **130**: 1075–1102.

Clough SA, Davitt CSA, Thorpe AJ. 1996. Attribution concepts applied to the omega equation. *Q. J. R. Meteorol. Soc.* **122**: 1943–1962.

Cox BD, Bithell M, Gray LJ. 1997. Modelling of stratospheric intrusions within a mid-latitude synoptic-scale disturbance. *Q. J. R. Meteorol. Soc.* **123**: 1377–1403.

Cullen MJP. 1993. The unified forecast/climate model. *Meteorol. Mag.* **122**: 81–94.

Davies T, Cullen MJP, Malcolm AJ, Mawson MH, Staniforth A, White AA, Wood N. 2005. A new dynamical core for the Met Office's global and regional modelling of the atmosphere. *Q. J. R. Meteorol. Soc.* **131**: 1759–1782.

Davis CA, Emanuel KA. 1991. Potential vorticity diagnostics of cyclogenesis. *Mon. Weather Rev.* **119**: 1929–1953.

Demirtas M, Thorpe AJ. 1999. Sensitivity of short-range weather forecasts to local potential vorticity modifications. *Mon. Weather Rev.* **127**: 922–939.

Deveson ACL, Browning KA, Hewson TD. 2002. A classification of FASTEX cyclones using a height-attributable quasi-geostrophic vertical-motion diagnostic. *Q. J. R. Meteorol. Soc.* **128**: 93–117.

Emanuel KA. 1986. An air–sea interaction theory for tropical cyclones. Part I: Steady-state maintenance. *J. Atmos. Sci.* **43**: 585–604.

Emanuel KA, Rotunno R. 1989. Polar lows as arctic hurricanes. *Tellus* **41A**: 1–17.

Gray SL, Dacre HF. 2006. Classifying dynamical forcing mechanisms using a climatology of extratropical cyclones. *Q. J. R. Meteorol. Soc.* **132**: 1119–1137.
Gregory D, Innes P. 2005. 'Convection scheme, Version 5.' Unified Model documentation. Met Office, Exeter, UK.
Griffiths M, Thorpe AJ, Browning KA. 2000. Convective destabilization by a tropopause fold diagnosed using potential-vorticity inversion. *Q. J. R. Meteorol. Soc.* **126**: 125–144.
Hoskins BJ, McIntyre ME, Robertson AW. 1985. On the use and significance of isentropic potential vorticity maps. *Q. J. R. Meteorol. Soc.* **111**: 877–946.
Huo Z, Zhang D-L, Gyakum JR. 1999. Interaction of potential vorticity anomalies in extratropical cyclogenesis. Part I: Static piecewise inversion. *Mon. Weather Rev.* **127**: 2546–2561.
Joly A, Jorgensen D, Shapiro MA, Thorpe AJ, Bessemoulin P, Browning KA, Cammas J-P, Chalon J-P, Clough SA, Emanuel KA, Eymard L, Gall R, Hildebrand PH, Langland RH, Lemaître Y, Lynch P, Moore JA, Persson POG, Snyder C, Wakimoto RM. 1997. The Fronts and Atlantic Storm-Track Experiment (FASTEX): Scientific objectives and experimental design. *Bull. Am. Meteorol. Soc.* **78**: 1917–1940.
Kuo Y-H, Shapiro MA, Donall EG. 1991. The interaction between baroclinic and diabatic processes in a numerical simulation of a rapidly intensifying extratropical marine cyclone. *Mon. Weather Rev.* **119**: 368–384.
Miner T, Sousounis PJ, Wallman J, Mann G. 2000. Hurricane Huron. *Bull. Am. Meteorol. Soc.* **81**: 223–236.
Nielsen NW. 1997. An early-autumn polar low formation over the Norwegian Sea. *J. Geophys. Res.* **102**: 13955–13973.
Nordeng TE. 1990. A model-based diagnostic study of the development and maintenance mechanism of two polar lows. *Tellus* **42A**: 92–108.
Petterssen S, Smebye SJ. 1971. On the development of extratropical cyclones. *Q. J. R. Meteorol. Soc.* **97**: 457–482.
Plant RS, Craig GC, Gray SL. 2003. On a threefold classification of extratropical cyclogenesis. *Q. J. R. Meteorol. Soc.* **129**: 2989–3012.
Pomroy HR, Thorpe AJ. 2000. The evolution and dynamical role of reduced upper-tropospheric potential vorticity in Intensive Observing Period One of FASTEX. *Mon. Weather Rev.* **128**: 1817–1834.
Rasmussen E. 1979. The polar low as an extratropical CISK disturbance. *Q. J. R. Meteorol. Soc.* **105**: 531–549.
Rasmussen EA, Turner J. 2003. *Polar lows: Mesoscale weather systems in the polar regions*. Cambridge University Press: Cambridge, UK.
Snyder C, Lindzen RS. 1991. Quasi-geostrophic wave-CISK in an unbounded baroclinic shear. *J. Atmos. Sci.* **48**: 76–86.
Stoelinga MT. 1996. A potential vorticity-based study of the role of diabatic heating and friction in a numerically simulated baroclinic cyclone. *Mon. Weather Rev.* **124**: 849–874.
Sundqvist H, Berge E, Kristjánsson JE. 1989. Condensation and cloud parameterization studies with a mesoscale numerical weather prediction model. *Mon. Weather Rev.* **117**: 1641–1657.
Wilhelmsen K. 1985. Climatological study of gale-producing polar lows near Norway. *Tellus* **37A**: 451–459.
Ziemianski M. 1994. 'Potential vorticity inversion.' Joint Centre for Mesoscale Meteorology (JCMM) Internal Report 39, 17 pp. University of Reading, Reading, UK.

DOI: 10.1002/qj